Marine Geology 326–328 (2012) 116–130

Contents lists available at SciVerse ScienceDirect

Marine Geology

journal homepage: www.elsevier.com/locate/margeo

# Effects of a major typhoon on sediment accumulation in Fangliao Submarine Canyon, SW Taiwan

Richard P. Hale [a,*], Charles A. Nittrouer [a], James T. Liu [b], Richard G. Keil [a], Andrea S. Ogston [a]

[a] School of Oceanography, University of Washington, Seattle, WA, USA
[b] Institute of Marine Geology and Chemistry, National Sun Yat-Sen University, Kaohsiung, Taiwan

ARTICLE INFO

*Article history:*
Received 29 December 2011
Received in revised form 6 April 2012
Accepted 19 July 2012
Available online 2 August 2012

Communicated by J.T. Wells

*Keywords:*
submarine canyon
hyperpycnal flow
sediment transport
flood
typhoon
Morakot
Taiwan

ABSTRACT

The Fangliao submarine canyon cuts across the shelf and slope of southwest Taiwan. Unlike other canyons along this margin, there is no obvious connection to an individual fluvial sediment source on land. Two recent cruises to Fangliao Canyon provide insight into sedimentation associated with a major typhoon. Box and piston cores were retrieved from Fangliao Canyon in early January 2007, after a local earthquake and an extended period of low-to-moderate river flow in streams that are suspected of contributing sediment to the canyon. Similar cores were collected from the canyon in early October 2009, following one of the largest typhoons to hit Taiwan in the past several decades. Typhoon Morakot delivered several meters of rain to Taiwan, with the largest river floods occurring in the south and southwest regions. In addition, the coastal ocean environment was energized by significant wave heights (>12 m).

Comparisons of textural, radioisotopic, and geochemical data reveal likely sediment transport and depositional processes within and surrounding Fangliao Canyon. Typhoon Morakot caused a layer ~10 cm thick (and greater) throughout the canyon. X-radiographs of the 2007 cores show limited physical structure in most cases, and the 2009 radiographs display obvious changes in sediment density relative to the underlying sediment, as well as distinct physical lamination. Examining signals from different geochemical and radiochemical tracers for terrestrial sediment source indicates that the flood layer deposited by Typhoon Morakot came from several small mountainous rivers. By comparing the results of the 2007 cruise with those from 2009, we gain significant insight to the close linkage between a line source of fluvial sediment and deposition in a submarine canyon, as well as the role that tropical-storm events can play in delivering sediment to these environments.



## 1. Introduction

Submarine canyons commonly serve as conduits for sediment, including organic carbon and other geochemical components, moving from a terrestrial source to a deep-ocean sink (Liu and Lin, 2004). The modern high stand of sea level has disjoined many canyons from their riverine sources, resulting in drastically reduced sediment transport and accumulation within canyons. This is not to say, however, that all canyons are disconnected from their sediment sources at present. Narrow continental shelves typically associated with tectonically active continental margins allow for connection between riverine source and deep marine sink, as can be seen in a range of submarine canyons (e.g.: Cap de Creus Canyon, DeGeest et al., 2008; Eel Canyon, Mullenbach et al., 2004; Gaoping Canyon, Liu et al., 2002; Monterey Canyon, Paull et al., 2005; Sepik Canyon, Walsh and Nittrouer, 2003). Canyons located proximal to their riverine sources are often characterized by gravity-flow deposits and non-steady-state accumulation, because the canyon serves as an efficient trap for material episodically reaching the continental slope (Huh et al., 2009; Liu et al., 2009). The sediment supply comes either directly from the river as a hypopycnal (surface), or hyperpycnal (bottom) plume, or indirectly as material that has been deposited on the continental shelf, remobilized, and transported by subsequent storms in the form of fluid muds and nepheloid layers (Puig and Palanques, 1998).

The shelf and slope offshore of Taiwan present an excellent opportunity for studying submarine gravity flows. Rapid tectonic uplift results in steep hillslope gradients and easily erodible rocks (Hilton et al., 2008). Several hundred megatons of sediment are delivered each year to the oceans surrounding the island (Kao and Milliman, 2008). Furthermore, Taiwan is impacted by numerous tropical cyclones every year, which provide significant precipitation to the small mountain streams incising its axial mountain range. The small drainage basins associated with these streams result in rapid fluvial response to storms, and flooding streams quickly discharge sediment onto a shelf still energized by wave activity. While a clear sediment pathway exists

* Corresponding author at: School of Oceanography, University of Washington, 1503 NE Boat Street, Room 104 Ocean Teaching Building (OTB), Seattle, WA 98105, USA. Tel.: +1 4014193678.
*E-mail address:* rhale@uw.edu (R.P. Hale).

0025-3227/$ – see front matter © 2012 Elsevier B.V. All rights reserved.
http://dx.doi.org/10.1016/j.margeo.2012.07.008

for some canyons along the southwest coast (e.g., Gaoping River to Gaoping canyon (formerly spelled Kaoping)), other canyons have no clear fluvial source (e.g., Fangliao Canyon). It is unknown whether the latter canyons are active conduits for sediment transfer.

This study utilizes seabed cores collected in and around Fangliao submarine canyon on the southwest coast of Taiwan (Fig. 1), in order (1) to determine the impact of a major typhoon on sedimentation within Fangliao submarine canyon, (2) to assess sediment accumulation in this canyon, despite the lack of a clearly recognizable point source of sediment, and (3) to consider the effectiveness of flood layer indicators in this and other similar settings.

## 2. Background

### 2.1. Sediment gravity flows

Sediment gravity flows are well documented processes by which suspended particles move to and through submarine canyon environments. They occur when the density of a fluid parcel exceeds the density of surrounding seawater due to sediment in suspension, causing the parcel to move down bathymetric gradients driven by gravity. Sediment gravity flows can be triggered by both tectonic and climatic forcings and are thought to be especially common in submarine canyons, due to over-steepened canyon walls, high sediment supply rates from nearby rivers, and the role of canyons as natural traps for sediment transported on continental shelves (Kudrass et al., 1998; Kineke et al., 2000; Mullenbach and Nittrouer, 2000; Liu et al., 2009).

Submarine canyons, and especially canyon heads, are capable of accumulating massive volumes of sediment in a relatively unconsolidated state (Mullenbach and Nittrouer, 2000; Lee et al., 2007). External forcings such as earthquake-generated shaking, or differential pressure from large surface gravity waves can produce cyclic stresses sufficient to cause liquefaction in some sedimentary strata, which may lead to catastrophic failure of this material and generate debris flows and/or turbidity currents traveling downslope (Marshall, 1978; Malouta et al., 1981; Adams, 1984; Goldfinger et al., 2003; Puig et al., 2003; Lee et al., 2007). Depending on the specific mechanism driving liquefaction, return frequencies for these types of gravity flows can range from a single year (e.g., Monterey Canyon; Xu and Rosenfeld, 2004) to several centuries (e.g., Cascadia subduction zone; Goldfinger et al., 2003). The duration of an individual debris flow or turbidity current is typically on the order of minutes to days and, in the case of submarine slides, can transport large volumes of sediment (>100 $m^3$) thousands of kilometers and change seabed sedimentary conditions (Parsons et al., 2007; Talling et al., 2007). The 2006 doublet of magnitude 7.0 earthquakes off the SW coast of Taiwan (Pingtung earthquake) resulted in submarine landslides and turbidity currents in both Gaoping and Fangliao Canyons that transported sediment ~250 km offshore into water depths approaching 4000 m, and is thought to have coarsened the seabed in upper Fangliao Canyon (Hsu et al., 2008).

In addition to inducing debris flows via cyclic loading, the wave-orbital velocities resulting from large, long-period waves associated with oceanic storms can impact the seabed in water as deep as ~150 m and resuspend seabed material to concentrations >30 g $l^{-1}$ (e.g., Komar et al., 1972; Traykovski et al., 2000; Wiberg, 2000; Puig et al., 2004). In seawater, the suspended-sediment concentration must exceed ~10 g $l^{-1}$ before the material behaves as a gravity flow. These wave-supported fluid muds can flow under the influence of gravity across continental shelves and through submarine canyons for tens of kilometers (Eel shelf and canyon, Puig et al., 2004; Monterey shelf and canyon, Xu and Rosenfeld, 2004). Typical durations of wave-supported fluid muds are on the order of hours to days, and they can incorporate particles as large as coarse sands (Parsons et al., 2007).

If the suspended-sediment concentration of a river exceeds ~40 g $l^{-1}$, the resultant plume may become negatively buoyant (hyperpycnal) upon entering the ocean, plunging beneath seawater and moving near the bottom, as opposed to spreading across the sea surface as a hypopycnal plume (Mulder and Syvitski, 1995; Mulder et al., 2003; Warrick and Milliman, 2003). As with fluid muds, a hyperpycnal plume that intersects a canyon can continue down the canyon for tens of kilometers (Mulder et al., 2003). Hyperpycnal

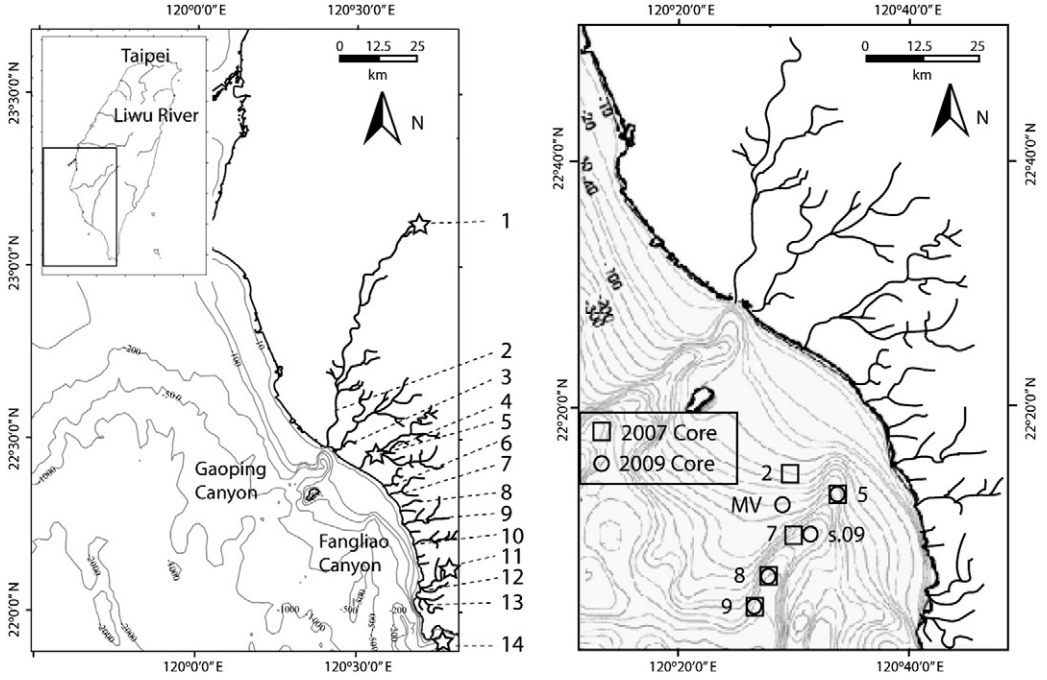


**Fig. 1.** Study area, SW Taiwan. Rivers and gauges as follows: (1) Nanfong gauge, (2) Gaoping River, (3) Donggang River, (4) Linbian River, (5) Sinbei gauge, (6) Peishih River, (7) Shihwen River, (8) Nanshihhu River, (9) Fengshan River, (10) Fengkan River, (11) Shihmen gauge, (12) Sihchong River, (13) Paoli River, (14) Eluanbi Buoy. Core locations from 2007 represented by squares, 2009 by circles. For repeat sites, a single label is used for both cores.

plumes are typically short-lived, lasting hours to days, and are spatially variable, so documenting them in situ has proven exceptionally challenging (Milliman and Kao, 2005).

### 2.2. Gravity-flow deposits

Gravity flows depend on large volumes of sediment available for transport, and therefore their deposits share many similarities with flood deposits. Gravity-flow deposits on continental margins typically are characterized by a higher degree of physical stratification than found in deposits formed during more quiescent conditions (Wheatcroft and Borgeld, 2000). This is due in part, to the observation that bioturbation is typically more effective at disturbing physical features left by sediment deposited during less-concentrated flow conditions (Nittrouer and Sternberg, 1981). If the gravity flow is generated by high-concentration river discharge, the deposit generally will exhibit an increase in clay fraction and organic carbon content, reflecting river sediment characteristics (Milliman and Meade, 1983; Leithold and Hope, 1999; Leithold and Blair, 2001). Deposits resulting from wave-supported gravity flows have also been shown to exhibit an increase in clay content, which may be coincident with increased sediment supply that occurs during river floods (Sommerfield et al., 1999; Mullenbach and Nittrouer, 2000). The combination of fine-grained sediment and rapid deposition results in decreased bulk density within a flood layer, relative to underlying pre-existing material (Wheatcroft et al., 2007). This transition should appear in x-radiographs obtained soon after gravity-flow deposition. Over time, physical and biological mixing reworks event deposits, modifying their signature; however increased clay content remains a useful indicator of past events (Drake, 1999).

When sediment particles are able to interact with seawater, they accumulate a radioisotopic signature with high activities of excess $^{210}$Pb. $^{210}$Pb ($t_{1/2}$ = 22.3 y) serves as a valuable tool for investigating sedimentation on timescales of 4–5 times its half-life (~100 y). A steady supply of sediment through the water column results in a logarithmic activity profile in the seabed (Nittrouer et al., 1979). Under these conditions, the dissolved $^{210}$Pb adsorbed by sediment particles is directly related to sediment surface area, which means it is inversely related to grain size (Nittrouer et al., 1979). In contrast, non-steady-state supply of sediment results in irregular $^{210}$Pb activity profiles, from pulsed deposition of new material (e.g., Alaskan shelf, Jaeger et al., 1998; Amazon shelf, Dukat and Kuehl, 1995; Gaoping submarine canyon, Liu et al., 2009). Within non-steady-state deposition, low levels of activity are interpreted as periods of rapid sediment input, when either the material does not interact sufficiently with the surrounding waters to scavenge a significant $^{210}$Pb activity and/or the concentration of material in suspension is more than sufficient to scavenge most $^{210}$Pb from the seawater contacted, thereby reducing the radioactivity on individual particles.

Sediment recently delivered by rivers usually carries a signature of radioactive $^{7}$Be, which is a naturally occurring, short-lived radioisotope ($t_{1/2}$ = 53 days), washed off land surfaces by rainfall. Therefore, $^{7}$Be can be a useful tool to establish a terrestrial source for recently deposited material (Sommerfield et al., 1999).

In addition to radioisotopic signatures, a suite of geochemical tracers can help establish the source of organic material in sediments from offshore cores. $\delta^{13}$C values allow for the identification of terrestrial material supplied to the marine environment. Terrestrial and marine plants have different pathways during photosynthesis, which distinguishes the fractionation of their stable-carbon isotopes. As a result, material entering the ocean from the land tends to have a more negative $\delta^{13}$C ratio of approximately −26.00‰, while marine organic carbon is typically between −20.00 and −22.00‰ (Degens, 1969; Liu et al., 2006). Organic signatures of discrete discharge events may be preserved in the seabed, so long as subsequent mixing does not obscure them, and the carbon is not remineralized. The ratio of nitrogen to carbon may be used in conjunction with the $\delta^{13}$C signature, to distinguish between soil and vascular plant debris. Soil tends to have an N:C ratio between 0.12 and 0.16, while vascular plant debris has a ratio of ~0 (Keil et al., 1994; Walsh et al., 2008).

Lignin compounds are found almost exclusively in vascular plant tissue (Sarkanin and Ludvig, 1971). As a result, these phenolic polymers can be useful for determining the fraction of terrestrial-sourced sediment in a marine environment (Hedges and Mann, 1979). The process of extracting and identifying the lignin phenols yields a suite of geochemical indicators, including acids and aldehydes. Acid to aldehyde ratios (Ad/Al) are a proxy for diagenesis, and can be used to determine the degree of degradation for organic material. If a sample is comprised of terrestrial material, the state of degradation can indicate whether the sample came from the soil surface or a deeper horizon, and can imply the extent of erosion associated with the sediment source. As a sample becomes more degraded, aldehydes are converted into acids, thereby increasing the Ad/Al ratio. Soil samples, for example, tend to have higher Ad/Al ratios than leaves or grasses. The ratio of cinnamyl to vanillyl phenols (C/V) commonly co-varies with Ad/Al, and is another potential indicator of material degradation or source.

### 2.3. Regional setting

Precipitation in Taiwan is strongly seasonal, with the overwhelming majority of precipitation occurring during the boreal summer. Taiwan as a whole receives an average of 250 cm of rain annually, although this varies by region from 160 to 800 cm due to orographic effects. The majority of Taiwan's precipitation is associated with typhoons, three to four of which impact Taiwan annually. Typhoons can bring extreme precipitation (>250 cm from a single storm in isolated areas), strong winds (>60 m s$^{-1}$), and great wave heights (>15 m; Doong et al., 2009). These strong climatic signals commonly lead to conditions conducive for gravity-flow generation from many Taiwan rivers, including the Choshuei, Gaoping, and Tsengwen (Mulder and Syvitski, 1995; Dadson et al., 2005; Chiang and Yu, 2008; Kao and Milliman, 2008).

Fangliao Canyon is located off the southwest coast of Taiwan, with the canyon head intersecting the shelf at the 50-m isobath, ~10 km from the coast. This canyon is approximately 30 km long with limited meandering (Fig. 1), and reaches depths of 1000 m where it enters Luzon Strait and merges with the Gaoping canyon, which extends into the Manila Trench. Fangliao Canyon was formed as one of many structural deformations in the Taiwan accretionary wedge associated with the tectonic evolution of the arc-continent collision between the Chinese continental margin and the Taiwan orogen (Liu et al., 1997). Unlike the nearby Gaoping Canyon (~25 km to the northwest, Fig. 1), which is directly connected to the Gaoping and Donggang rivers, Fangliao Canyon has no obvious connection to an extant river. The small mountain streams located to the north and east of Fangliao Canyon have drainage basins of 100–1000 km$^2$, with estimated peak water discharges of ~100 m$^3$ s$^{-1}$ (Chang, 1983). Discharges from these basins vary seasonally, and are controlled by the frequent tropical storms described above.

### 2.4. Typhoon Morakot

The 2009 typhoon season began relatively slowly in Taiwan, with no storms making landfall in the first 3 months. Taiwan felt the effects of Typhoon Linfa (Cat 1 classification) in June and Tropical Depression Huaning in July, though neither storm led to exceptionally prolonged or intense rainfall (Kao et al., 2010). In August, however, Taiwan was ravaged by Typhoon Morakot. The maximum sustained winds were ~42 m s$^{-1}$, corresponding to a strong category 1 hurricane. Typhoon Morakot's major impact was through flooding, especially on the southern half of the island. During 7 days, the storm delivered

>270 cm of rain to some high-mountain regions, including the headwaters of the small rivers along the southwest coast of Taiwan (Fig. 2). The associated flooding resulted in massive landslides and intense river mobilization (e.g., migration and incision; Lang, 2009). In some areas, waves associated with Typhoon Morakot had heights >13 m and periods ~12 s (Doong et al., 2009).

## 3. Methods

### 3.1. Sample collection

Box core samples were collected from two cruises aboard the R/V Ocean Researcher 1 in January 2007 (cruise 820) and September/October 2009 (cruise 915). Ten box cores were collected in 2007 (8 presented in this paper), and subsampled with 10-cm-diameter PVC core barrels, which were transported back to the lab and kept in cold storage. They were cut in half lengthwise, and sampled at 1-cm intervals for subsequent analyses. Six box cores were collected in 2009 and were subsampled with 10-cm-diameter PVC core barrels, which were immediately sectioned into 1- and 2-cm intervals onboard the ship. Samples were bagged and placed in cold storage for subsequent analyses. In addition, push-core x-ray trays (30 cm long × 12 cm wide × 4 cm thick) were inserted into each box core, for x-ray imaging immediately upon return to shore. Of the cores collected in 2009, two cores (915–8, 915–9) were reoccupations of 2007 sites (820–8, 820–9), and a third core (915-s.09) was obtained close (~1500 m) to another 2007 station (820–7) (Fig. 1, Table 1).

River-water and suspended-sediment samples were collected throughout Typhoon Morakot from the Liwu River in northeast Taiwan. The Liwu River is a deeply incised mountain river, which

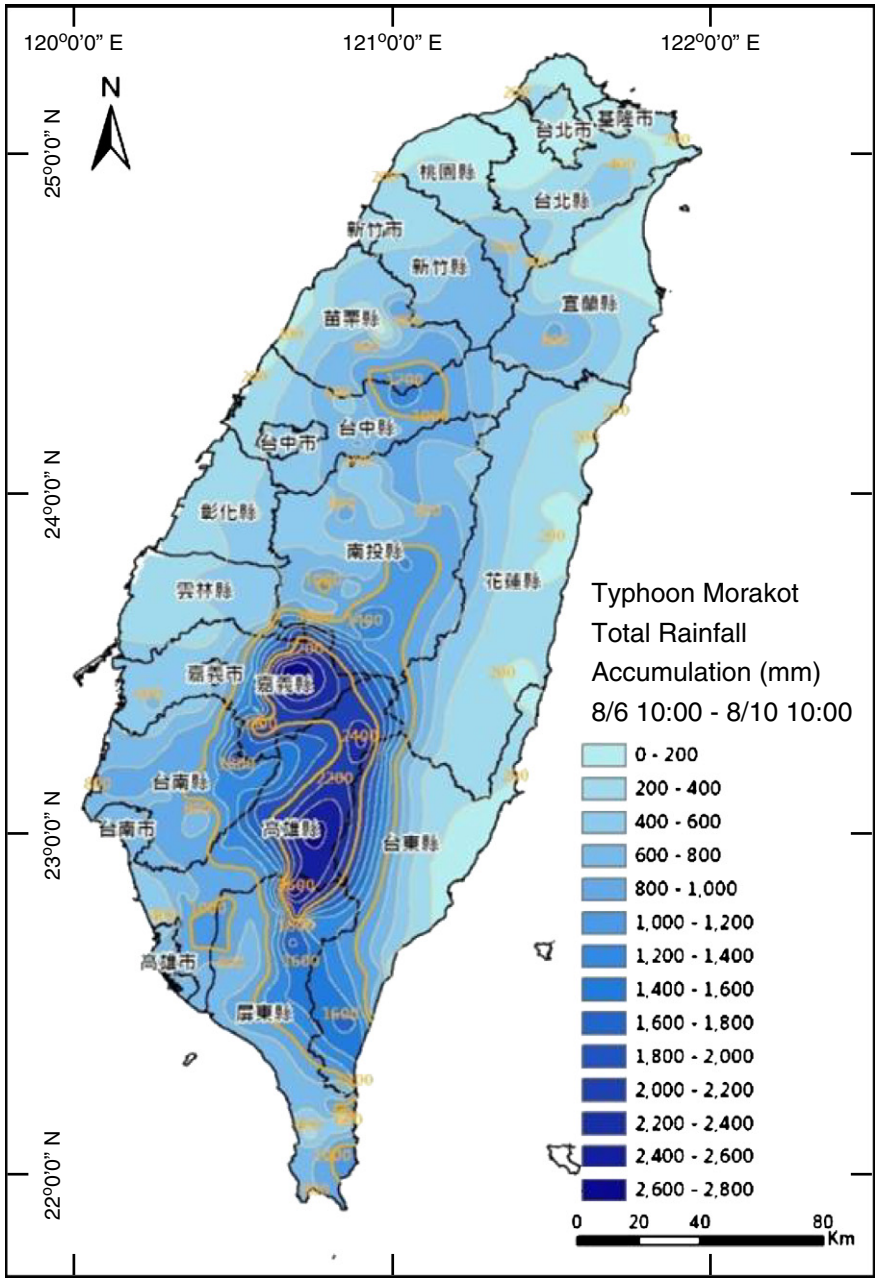


**Fig. 2.** Precipitation totals during Typhoon Morakot. Notice that the highest rainfall totals occurred partially in the northern extent of the drainage basins associated with the study area (from Central Geological Survey, Ministry of Interiors, ROC).

**Table 1**
Locations and depths of cores analyzed in this study.

| Core ID | Latitude (°E) | Longitude (°N) | Depth (m) | Location |
|---|---|---|---|---|
| *2007* | | | | |
| OR1-820-1 | 22.2499 | 120.5100 | 120 | Shelf |
| OR1-820-2 | 22.4900 | 120.5328 | 140 | Shelf |
| OR1-820-3 | 22.2841 | 120.5435 | 45 | Shelf |
| OR1-820-5 | 22.2284 | 120.5693 | 383 | Canyon head |
| OR1-820-7 | 22.1676 | 120.5264 | 690 | Thalweg |
| OR1-820-8 | 22.1096 | 120.4798 | 826 | Thalweg |
| OR1-820-9 | 22.0677 | 120.4609 | 864 | Thalweg |
| OR1-820-18 | 22.9900 | 120.4805 | 800 | Canyon flank |
| *2009* | | | | |
| OR1-915-MV | 22.2096 | 120.4861 | 324 | Shelf |
| OR1-915-5 | 22.2284 | 120.5693 | 361 | Canyon head |
| OR1-915-s.09 | 22.1676 | 120.5246 | 657 | Thalweg |
| OR1-915-8 | 22.1093 | 120.4795 | 825 | Thalweg |
| OR1-915-9 | 22.0672 | 120.4593 | 859 | Thalweg |

intersects the east coast of Taiwan ~15 km north of the town of Hualien (Fig. 1). The Liwu River does not drain into the study area; however, it is used in this case as an example of small mountainous streams (drainage basin ~620 km$^2$) like those along the SW coast of Taiwan. The Liwu River is located on the northern half of Taiwan, which saw significantly less precipitation associated with Typhoon Morakot than did the southern half of Taiwan, where Fangliao Canyon is located. Approximately 5 km upstream of its mouth, the Liwu transforms to a braided river. Samples were collected from a bridge ~5 km from the river mouth by lowering a rack of four, 1-L bottles into the raging surface waters until all four bottles were full. Sample collection began on 6 August 2009, ~6 h before the arrival of the storm impact, and continued every 3 h for 72 h, capturing the peak discharge and the onset of waning flow. Suspended-sediment concentrations from these samples were determined by evaporating the known volume of water and weighing the remaining, dried sediment.

### 3.2. Sedimentological analysis

Cores collected in 2007 were opened in October 2008. One half of the core barrel was preserved as an archive, and a PVC x-ray tray (25 cm × 8 cm × 1 cm) was inserted into the other half. Each extracted core section was x-rayed in June 2009 using an Associated X-ray Corporation Minishot MI160NH. Because of the time between core collection and x-ray imaging, moderate desiccation had occurred and the sediment had cracked in several places, as is evident in the radiographs (Figs. 3–6). The push-core trays collected on the 2009 cruises were x-rayed using the same system, immediately upon arrival in port. By shortening the time interval between collection and imaging, we were able to obtain significantly higher-quality x-radiograph images from the 2009 cores.

Textural analyses were used to normalize radionuclide activity for particle size, as well as provide insight to conditions during sedimentation. Subsamples were obtained at intervals of 1–5 cm, and analyzed using a method modified from that described by Mullenbach and Nittrouer (2000). Dispersant solution ($NaPO_3$) was added to homogenized subsamples, which were subsequently sonicated in a water bath for >15 min. Samples were then sieved at 4 phi to separate fine-grained and coarse-grained fractions. The fine-grained fraction was analyzed using a Micromeritics Sedigraph to determine the grain-size distribution within the mud fraction (Coakley and Syvitski, 1991). Dry weights of the coarse-grained and fine-grained fractions were used to determine the relative fractions of sand versus mud.

### 3.3. Geochemical analysis

$^{210}$Pb activities for all cores were established via alpha spectroscopy, using a version of the method developed by Nittrouer et al. (1979). Assuming $^{210}$Pb and its effective daughter $^{210}$Po exist in secular equilibrium, measuring the alpha decay of $^{210}$Po allowed for the determination of $^{210}$Pb activity. Dried, crushed samples were spiked with a known activity of $^{209}$Po (a human-produced isotope) to determine yield. $^{210}$Po and $^{209}$Po were then chemically separated from the sediment by successive leachings with 16 N $HNO_3$ and 6 N HCl. These isotopes were collected on silver planchets suspended in the leachate for 24 h, and the silver planchets were counted for alpha decay.

Excess $^{210}$Pb activity was calculated by subtracting the supported level of $^{210}$Pb activity from the total measured $^{210}$Pb activity. Supported activities are maintained by the *in situ* decay of its effective parent, $^{226}$Ra, and were calculated from deep portions of cores where the profile of total activity becomes low and uniform. In cases of steady-state deposition, $^{210}$Pb activity profiles can be characterized by a logarithmic decrease downward that ultimately reaches the supported level. The slope of the excess-$^{210}$Pb line in the region of logarithmic decay can be used to determine sediment accumulation rates (Nittrouer et al., 1979).

All cores collected in 2009, as well as the samples obtained from the Liwu River, were examined for $^{7}$Be activity with a method modified from that described by Sommerfield et al. (1999). Core samples were dried for several days at 60 °C to calculate water content, which was used to determine the dry-bulk density. In the case of the sediment cores, a correction was made for the residual salt mass. Samples were then crushed and 20–60 g was placed in 60-ml, polyethylene counting vessels. $^{7}$Be activity was determined from the 477.6-keV peak of the planar gamma-decay counter.

Total carbon, total nitrogen, and $\delta^{13}$C analyses were measured on four cores (915–9, 915–8, 915-s.09, 915-MV) collected in 2009. 30–50 mg of dried, crushed, acidified sample were sent to the Stable Isotope Lab at University of California, Davis for analysis via mass ratio spectrometry. Lignin phenols from several 2009 cores were quantified after using the cupric oxide oxidation method described by Goni and Hedges (1990). Ethyl ether was used to extract the acidic CuO reaction products of dried, crushed samples oxidized under basic conditions (8% NaOH) and high temperature (155 °C). The reaction products were then analyzed as trimethylsilyl derivatives (*N,O*-Bis(trimethylsilyl)trifluoroacetamide, Regis Chemical Co.) by gas chromatography mass spectroscopy. A known volume of ethylvanillin was used as a recovery standard to quantify lignin phenols from individual compounds.

### 3.4. Riverine and oceanic data

Daily river water and sediment discharge records from all gauging stations operated by the Taiwanese Central Weather Bureau proximal to the study site were examined, going as far back as the 1970's when available. The rivers (and stations) are listed in Table 2, and include: Gaoping (Liling and Nanfong), Donggang (Chaojhou), Linbian (Sinbei), and Sihchong (Shihmen). Unfortunately, the flood associated with Typhoon Morakot was so great that it not only destroyed several river gauges, it also overwhelmed the capacity of the rating curve to accurately estimate suspended-sediment concentrations during the storm. To determine if the recorded maximum water discharges were reliable, we compared them to the maximum theoretical discharge based on drainage area, using the method described by Matthai (1990). The correlation in timing between peak river discharge and oceanographic conditions was assessed by examining hourly wind and wave data from a buoy off the southern peninsula of Taiwan (Fig. 1) during Typhoon Morakot and the following months. Wind directions were evaluated in order to establish whether conditions

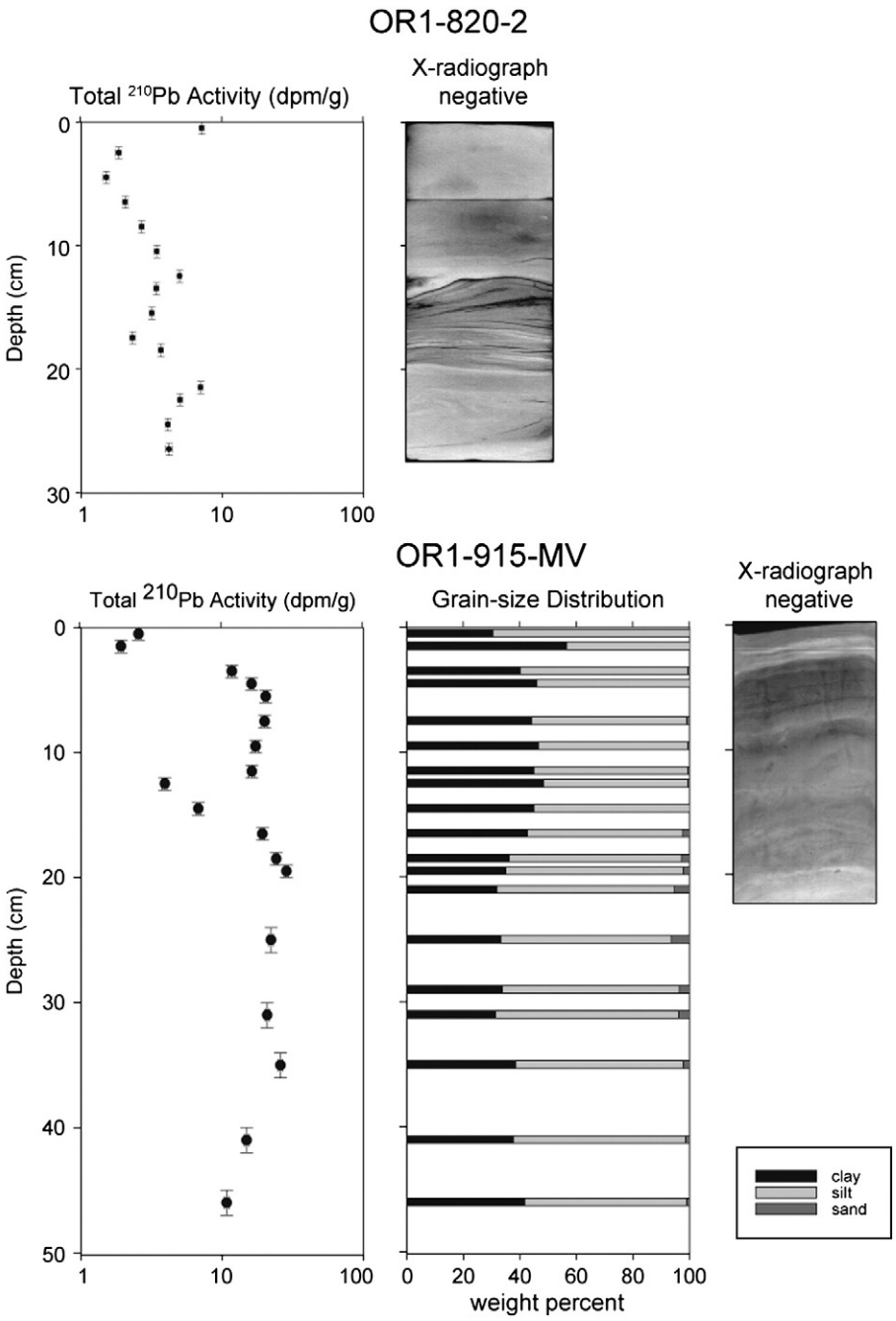


**Fig. 3.** Cores collected on the continental shelf during 2007 (ORI-820-2) and 2009 (ORI-915-MV). Note the variable $^{210}$Pb activities – evidence for non-steady-state deposition. ORI-820-2 shows evidence for wave activity in the form of wavy bedding from 10 to 15 cm. The surface 2–4 cm of ORI-915-MV displays physically stratified beds truncating a bioturbated bed.

were favorable for upwelling or downwelling. Wavelength estimates were made based on wave periods, and linear wave theory was used to estimate the impact of the waves on the shelf bottom.

## 4. Results

### *4.1. Sedimentary structures*

Desiccation of cores collected in 2007 made detailed event identification difficult; however, evidence is seen for three different types of physical structure: wavy bedding, horizontal laminae (mm to cm thicknesses), and massive bedding (Figs. 3–6). Cores 820–1 and 820–3 (shelf) are massively bedded in x-radiographs. Core 820–2 (shelf edge) displays wavy-flaser bedding in the region 10–15 cm (Fig. 3). Cores 820–5 (canyon head, not presented) and 820–7 (midway down canyon axis; Fig. 4) show fine horizontal laminae (mm to cm thicknesses). Core 820–8 (canyon thalweg) displays mm-scale laminae throughout the core, with 3 cm of non-laminated material and higher bulk density at the surface (Fig. 5). Core 820–9 (canyon thalweg) also displays material with high bulk density (4–10 cm, 30–32 cm), but is otherwise massive (Fig. 6). Core 820–18 (distal end of canyon, not presented) shows mm to cm scale laminae.

Cores collected in 2009 provided much clearer x-radiograph images. Every core collected in Fangliao Canyon has a surface layer (3–12 cm) of high porosity, physically stratified sediment overlying more consolidated strata (Figs. 3–6). The surface low-density layer shows no evidence of bioturbation, although in several cores (915-MV, 915-s.09), the base of this layer truncates macrofaunal burrows. The

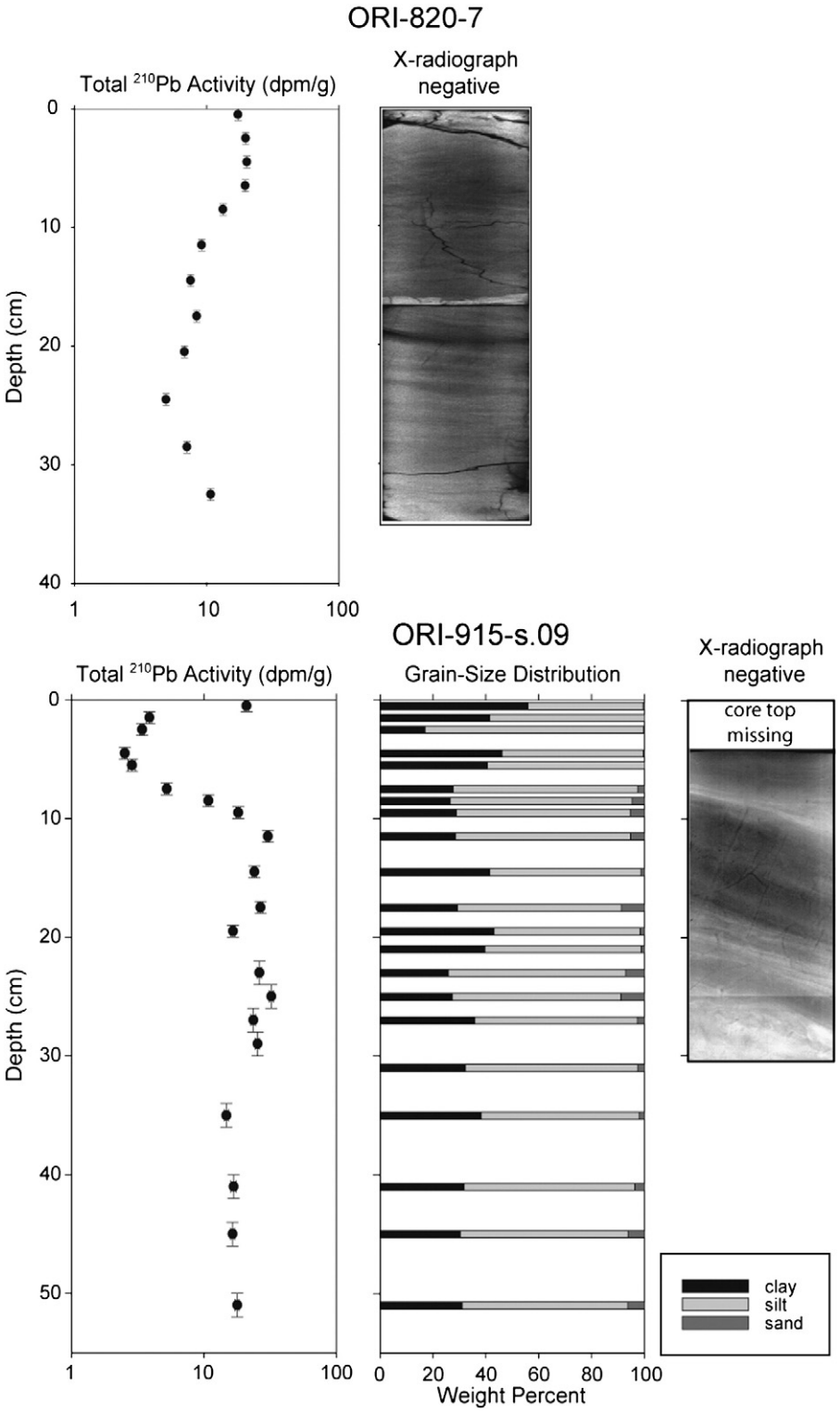


**Fig. 4.** Cores from the canyon thalweg approximately 13 km from the canyon head, collected in 2007 (ORI-820-7) and 2009 (ORI-915-s.09). ORI-820-7 shows evidence for non-steady-state accumulation, with the increase in $^{210}$Pb activity below 25 cm. ORI-915-s.09 shows very low $^{210}$Pb activities in the upper 10 cm, corresponding to a physically stratified layer which appears to truncate pre-existing burrows in x-radiograph.

surface layer is thinnest (3 cm) in core 915-MV, which is located on the continental shelf near the shelf break, and in core 820–2. Cores from the canyon display a trend of thickening surface layer with increased depth. This layer is ~7 cm thick at station 915-s.09, ~9 cm at station 915–8, and ~12 cm at station 915–9, located at 13, 21, and 26 km from the canyon head, respectively.

### 4.2. Grain size

Cores from both 2007 and 2009 display variations in grain size indicative of non-steady-state deposition. All cores are predominantly silt, which comprises 40–70% of the core mass. Cores 820–8 and 820–9 from the canyon thalweg show an increase in the sand fraction

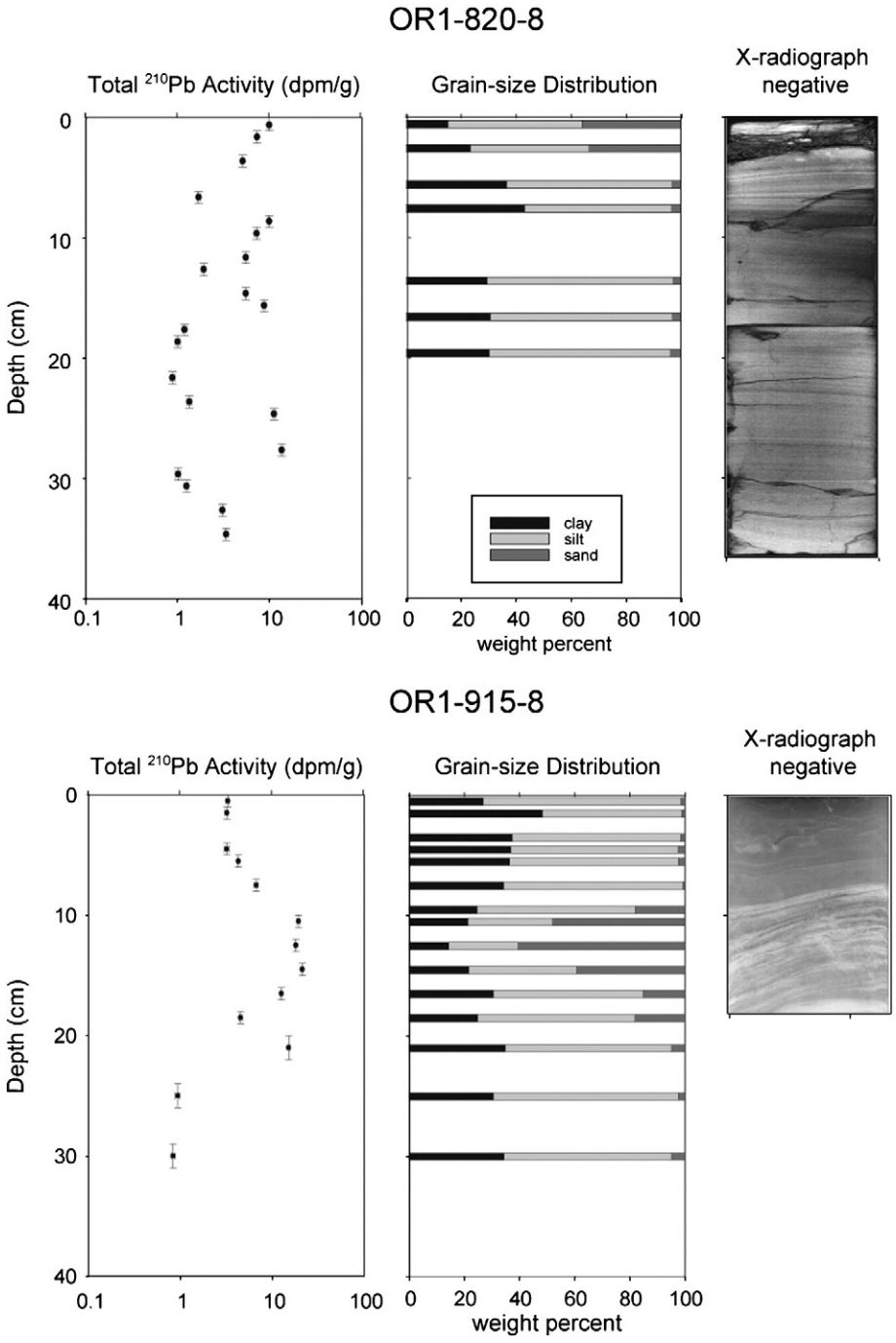


**Fig. 5.** Cores collected from the canyon thalweg 21 km from the canyon head in 2007 (ORI-820-8) and 2009 (ORI-915-8). $^{210}$Pb profiles from both cores exhibit non-steady-state accumulation, and physical stratification in x-radiographs. The surface layer of ORI-915-8 has low $^{210}$Pb activity, increased clay content, and is of lower bulk density than the underlying material. Note the gradual transition from high- to low-activity material between 12 and 6 cm, which possibly indicates mixing of shelf- and river- derived materials prior to delivery down canyon.

to as much as 30% by mass, coincident with the structures observed near the surfaces of the x-radiograph images (Figs. 3–6). Clay fractions range from 15% to 30% in these regions. The material in the deep layers of these axial cores ranges from 1% to 10% sand and 30% to 45% clay, by mass. In core 820–2 from the shelf edge, the sand fraction increases drastically for the region 10–15 cm, the same depth as the physical stratification observed in x-radiographs.

The surface layers observed in 2009 cores reveal significant fining in grain size compared with the underlying layers, and silt and clay are far more prevalent than in the underlying sandy beds. In core 915–8, the surficial 8 cm are characterized by 0.5–2.5% sand, and 25–50% clay. Immediately below this, lies 10 cm of material comprised of 15–60% sand and 15–30% clay. The other cores from the canyon thalweg exhibit the same trends, below the upper 12 cm of 915–9 and the upper 7 cm of 915-s.09. In general, the smallest percentage of sand and greatest percentage of clay are found in the upper 3–10 cm of each 2009 core.

### 4.3. Radioisotope signatures

Profiles of total $^{210}$Pb from most 2007 cores and all 2009 cores have alternating high- and low- activity layers, suggesting non-steady-state deposition (Figs. 3–6). Cores collected in 2009 show relatively low

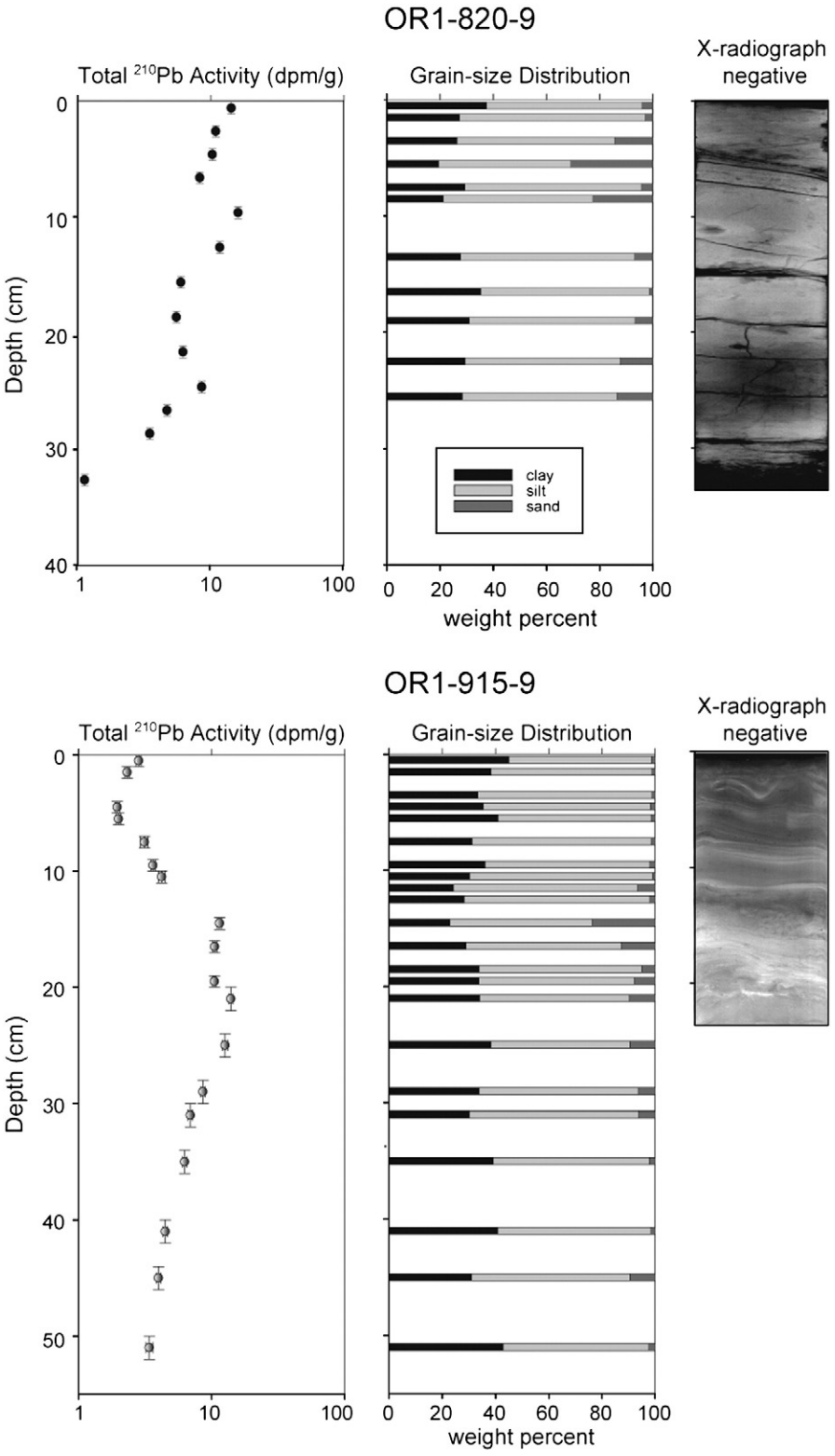


**Fig. 6.** Cores collected from the canyon thalweg 26 km from the canyon head in 2007 (ORI-820-9) and 2009 (ORI-915-9). $^{210}$Pb profiles from both cores exhibit non-steady-state accumulation, and physical stratification in x-radiograph. The surface layer of ORI-915-9 has low $^{210}$Pb activity, increased clay content, and is of lower bulk density than the underlying material. Note the gradual transition from high- to low-activity material between 14 and 6 cm, which possibly indicates mixing of shelf- and river- derived materials prior to delivery down canyon. Also, the coarse-grained layer near the surface of ORI-820-9 appears to correlate well with the coarse-grained layer underlying the surface material in ORI-915-9.

activities (<5.0 dpm $g^{-1}$) coincident with the physically stratified, finer-grained layers identified at the surface. The layers of low activity appear to be thicker within the canyon (stations 915-s.09, 915–8, 915–9; extending to 10–12 cm; Figs. 4–6) than on the shelf (station 915-MV; extending to 3 cm; Fig. 3), and appear to thicken with distance down canyon. Below the surface layer, total $^{210}$Pb activities resemble surface or near-surface activities from cores collected in 2007, 15–30 dpm $g^{-1}$, depending on the location. The variations in

**Table 2**
Drainage basin area and gauged (gray) and estimated (white) discharge from rivers proximal to Fangliao Canyon.

| River (station name) | Drainage basin area ($km^2$) | Gauged Morakot discharge ($m^3\ s^{-1}$) | Previous-known peak discharge ($m^3\ s^{-1}$) (year) | Maximum possible discharge (from drainage basin area) ($m^3\ s^{-1}$) |
|---|---|---|---|---|
| Gaoping River (Liling) | 3287 | 15,250 | 13,800 (1996) | 18,200 |
| Gaoping River (Nanfong) | 338 | 1300 | 630 (2006) | 6700 |
| Donggang River (Chaojhou) | 422 | 670 | 910 (1981) | 7500 |
| Linbian River (Sinbei) | 310 | 3000 | 1900 (1992) | 6400 |
| Sihchong River (Shihmen) | 130 | 420 | 130 (2001) | 4000 |
| Peishih River | 32 | Unknown | Unknown | 1700 |
| Shihwen River | 90 | Unknown | Unknown | 3200 |
| Nanshihhu River | 21 | Unknown | Unknown | 1300 |
| Fangshan River | 125 | Unknown | Unknown | 3900 |
| Fengkang River | 103 | Unknown | Unknown | 3500 |
| Paoli River | 104 | Unknown | Unknown | 3500 |

total $^{210}$Pb activity observed in these cores, however, are not obviously the result of grain-size variations (i.e., radioactivity does not vary inversely with grain size). With few exceptions (e.g., low activities at ~10–15 cm in 820–2; Fig. 3), grain-size distributions and total $^{210}$Pb activities are inversely related, with the finer material in the surface-stratified layer displaying relatively low total $^{210}$Pb activity. Because the profiles suggest non-steady-state accumulation, the standard method of calculating sediment accumulation rates from excess activity is not applicable. We can, however, estimate accumulation rates based on the observation of excess $^{210}$Pb activity at the base of most cores. For example, in the case of 915-s.09, we can see that the activity at the base (~50 cm) is less than one half-life lower than the maximum activity, suggesting an accumulation rate of $>2$ cm $y^{-1}$ (50 cm in <22.3 years; Fig. 6). This method is constrained by the core length, and the relatively short cores collected for this study provide minimum estimates of accumulation rates.

Cores from 2007 were not analyzed for $^{7}$Be, as they were processed after $^{7}$Be disappeared by decay. Cores from 2009 were analyzed for $^{7}$Be to depths of 15 cm, but $^{7}$Be was not detected above background levels in any of the cores. Similarly, river suspended-sediment samples obtained from the Liwu River during Typhoon Morakot do not reveal $^{7}$Be above background levels. Sediment samples from the river bank and suspended sediment from the river water collected on 25 August 2009 near the mouth of the Gaoping River were also below the detection limit for $^{7}$Be (Kao, S.J., pers. comm.).

### 4.4. Organic geochemistry

Samples for organic analyses were selected from specific horizons based on textural and radiochemical analyses. These horizons are: "surface" – the physically stratified, fine-grained, low $^{210}$Pb layer; "coarse" – the coarse-grained, high $^{210}$Pb activity layer underlying the surface layer, and; "bottom" – material from anywhere deeper in the cores (Fig. 7). To determine how much of the organic matter in the samples is of terrestrial origin, we used a simple two-end member mixing model (Hedges, 1976). The model requires that we define the marine end-member $\delta^{13}$C value, which we set to −21.5‰ based on Westerhausen et al. (1993) assessment of marine waters at similar latitude. The terrestrial end member is defined as the intercept of the lines relating organic carbon content to $\delta^{13}$C (Fig 8a). In this plot, the coarse and deep horizons have similar trends and are grouped together. The difference in the slopes of the lines indicates the relative amount of dilution in $\delta^{13}$C that occurs due to the addition of marine organic carbon (*sensu* Keil et al., 1997). The x-axis value where the two lines intersect indicates the initial average weight % of organic matter coming from land, and the intercept of the two lines denotes the original $\delta^{13}$C value of the terrestrial end member. This latter value is −25.5‰, consistent with the estimate (−26 ± 0.5‰) calculated by

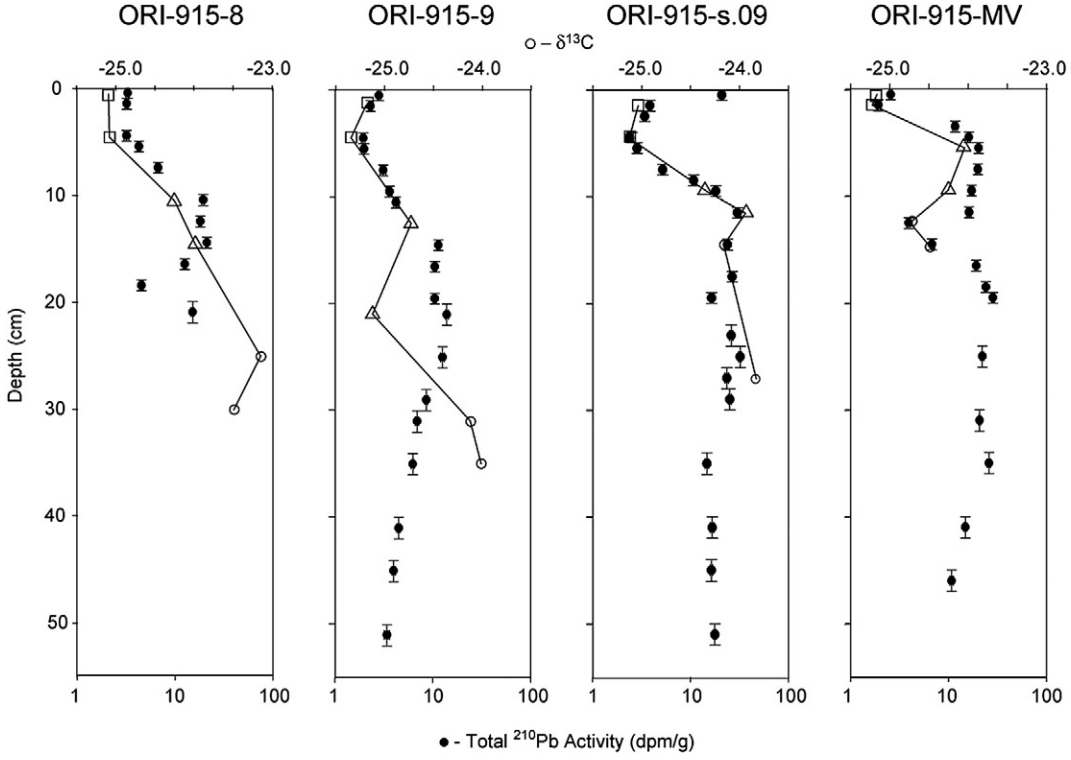


**Fig. 7.** Profiles of $^{210}$Pb (black dots) and $\delta^{13}$C (open shapes) from cores collected in 2009. "Surface" samples are open squares, "coarse" samples are open triangles, and "bottom" samples are open circles. −26.00‰ represents the terrestrial end member for carbon. Note the similar trends of $^{210}$Pb activity and $\delta^{13}$C, especially near the surface.

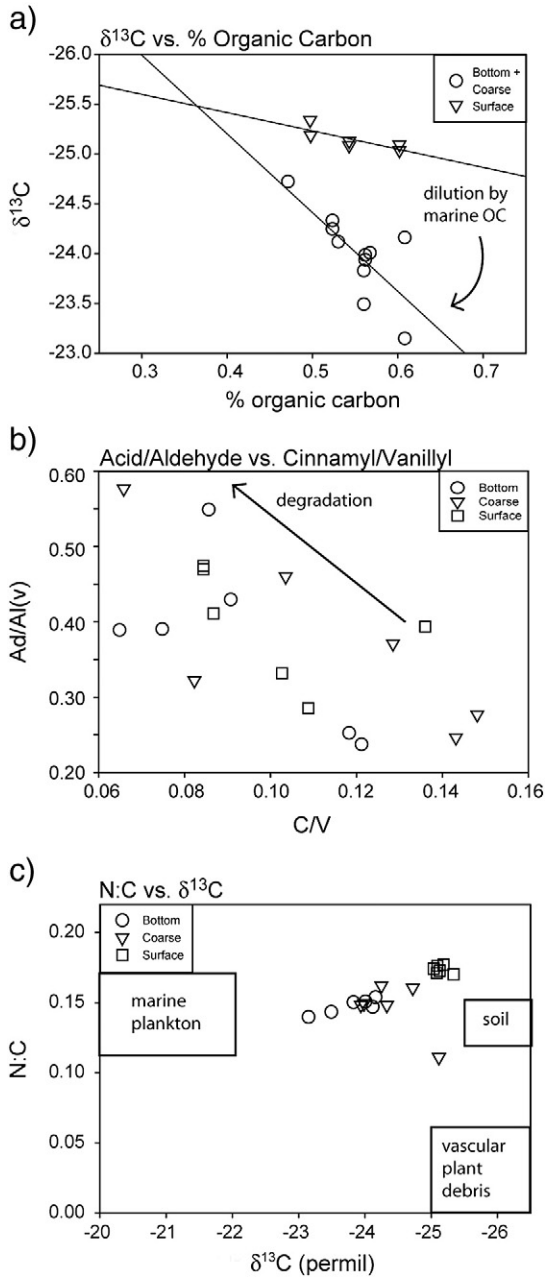


**Fig. 8.** Organic geochemical data, comparing (a) $\delta^{13}C$ and percent organic carbon, (b) acid:aldehyde ratio with carboxyl/vannilyl ratio, and (c) N:C ratio with $\delta^{13}C$. Samples were selected from three layers based on the results from textural and geochemical tools, as depicted in Fig. 7.

Kao and Liu (2000) for Taiwanese forests. Using these end-member values, the organic portions of the bottom and coarse samples are $65 \pm 13\%$ and $71 \pm 7\%$ terrestrial, and the surface samples are significantly enriched in terrestrial source (Student's *t*-test, $p<0.001$) at $92 \pm 2\%$. Sediments typically delivered to the marine system carry approximately 0.4 wt.% organic carbon, and material in the surface sediments is 20–50% more terrestrial.

Lignin phenol and elemental data can be used together to evaluate the character of the organic matter in the three horizons. We focus on the results from three comparisons: Ad/Al versus C/V ratios, $\delta^{13}C$ versus percent organic carbon, and nitrogen:carbon versus $\delta^{13}C$ (Fig. 8). Ad/Al ratios increase as lignin is degraded and range from 0 (fresh wood) to >3.0 (Hedges, 1976; Keil et al., 1998). In our system, they vary between 0.2 and 0.6, indicative of relatively fresh or mildly degraded material (Keil et al., 1998). C/V ratios indicated changes in the source of the lignin (high C/V ratios indicate contributions from non-woody parts of trees and grasses) as well as a change in degradation (low C/V values can result because cinnamyl phenols are preferentially degraded). There are no significant differences in these parameters between the surface, coarse and deep sediment horizons, and the terrestrial organic matter present in the system is primarily leaf or grass-derived material undergoing early diagenesis (Fig. 8b). The data can further be used to discriminate between marine material and terrigenous material that is either fresh or has spent time in soils (Fig. 8c; Keil et al., 1994; Walsh et al., 2008). Given end-member values for N:C (from Walsh et al., 2008) and $\delta^{13}C$ end members described above, the deep and coarse horizons contain terrestrial organic matter that is a mixture of marine material and soil while the surface samples cluster closer to the soil end member (Fig. 8c). Overall, these organic characterizations indicate that the source of organic matter to the surface horizon is >90% terrestrial organic matter that is derived from soil and is not significantly diluted by additional marine inputs.

### 4.5. Riverine and oceanic conditions

Prior to the storm, river discharge at all gauging stations was low; on the order of tens of $m^3\ s^{-1}$. All rivers reached their peak discharge during 8–9 August 2009 (Fig. 9). Peak recorded discharges were on the order of $10^2$–$10^3\ m^3\ s^{-1}$ for the rivers north and east of Fangliao Canyon, and an order of magnitude larger (~$10^4\ m^3\ s^{-1}$) for Gaoping River (Fig. 9, Table 2). From the three stations that did not fail during the storm, we see that discharge returned to its pre-storm levels by 11–13 August. The peak recorded discharges are 10–50% of their theoretical maxima (based on drainage basin, after Matthai, 1990; Table 2), so water-gauge-determined water discharges are considered reasonable. The sediment-rating curves are overwhelmed by the flood signal, but suggest suspended-sediment concentrations on the order of hundreds of grams per liter.

Typhoon Morakot generated energetic ocean conditions off the southwest coast of Taiwan. Examinations of hourly wind and wave data (Fig. 9) from the Eluanbi wave buoy (Fig. 1) demonstrate that wave heights increased from ~1–2 m to >10 m during 8–9 August, then returned to ~1–2 m by 14 August. Waves remained <5 m through October, with two smaller, discrete wave events. Associated with the increase in wave height during ~9–14 August was a shift in wave direction. Immediately before typhoon Morakot, the dominant wave direction was from the southeast at ~130° (nearly parallel to the southwest coast). Waves shifted to the south and southwest during 4–14 August, ranging from 190 to 240° (perpendicular to the southwest coast). After the storm, waves shifted back to the south and east, ~90–180°.

Sustained winds at an anemometer located three meters above the water surface initially decreased from ~10 $m\ s^{-1}$ to <5 $m\ s^{-1}$ on 3 August, before increasing to ~25 $m\ s^{-1}$ by 8 August. By 15 August, winds had decreased again to ~5 $m\ s^{-1}$. As with wave direction, wind direction shifted during Typhoon Morakot. Winds were from the east-northeast (5°) until 3 August, at which point they rotated clockwise to the west northwest (290°) by 5 August. Direction remained relatively constant until 7 August, when it changed to the west southwest (240°), and remained until 14 August. After that, winds were light and variable, or relatively weak with a generally easterly direction, ranging from 50° to 100°.

## 5. Discussion

### 5.1. Evidence of flood deposit

Sedimentological and geochemical evidence suggests that between January 2007 and October 2009, a major event impacted the seabed and deposited a layer of sediment on both the shelf and in Fangliao Canyon. While several storms passed over Taiwan during this period, the wettest, by far, was Typhoon Morakot in August, 2009. X-radiographs collected on

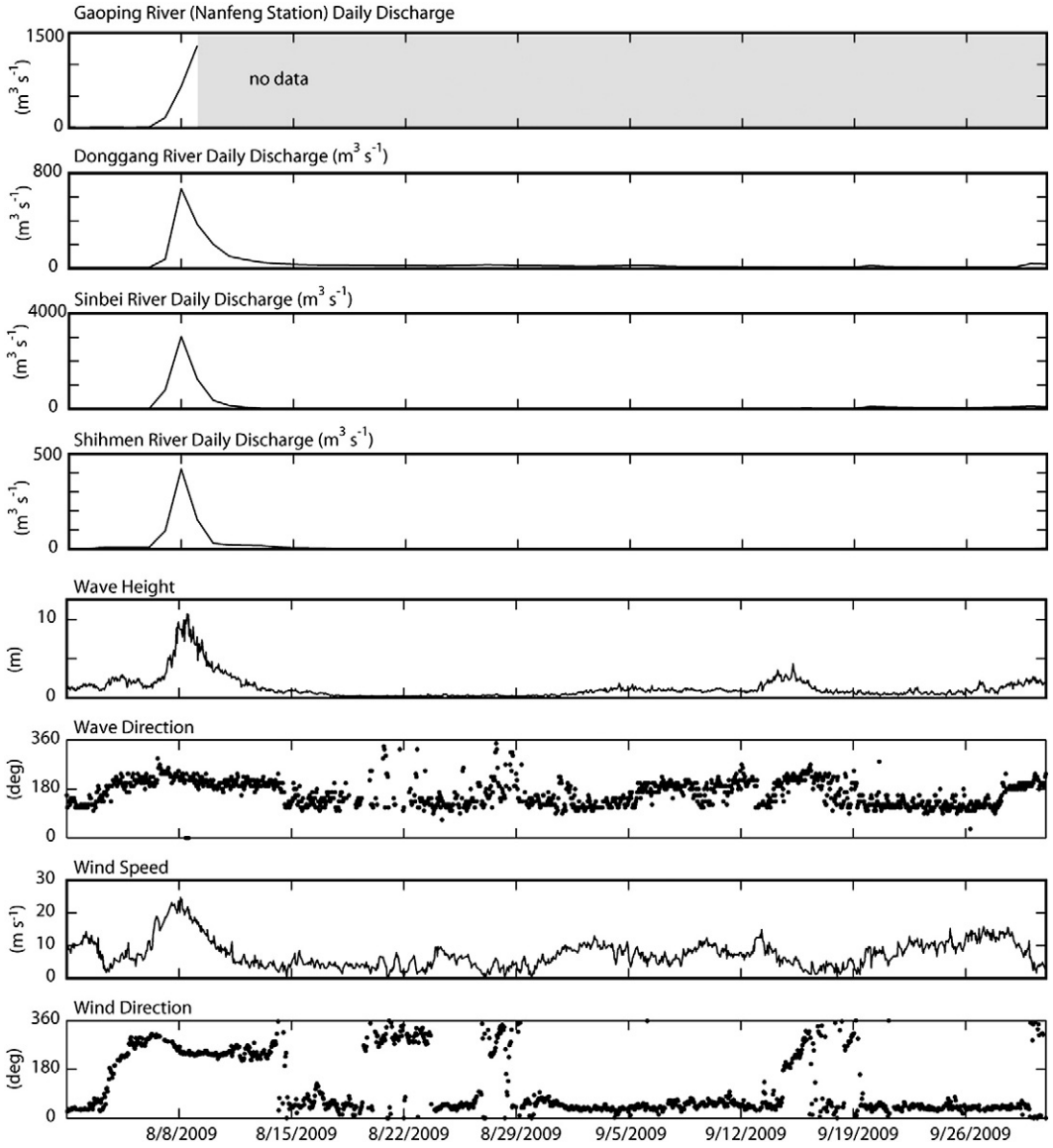


**Fig. 9.** Daily water discharge from tributaries to Gaoping Canyon (Nanfeng station and Chao Chou River), Fangliao Canyon (Hsin Pei and Shihmen Rivers), and hourly meteorological data from Eluanbi wave and weather buoy during Typhoon Morakot and the ensuing weeks. Peak discharge coincided with peak wave height (>10 m), peak wind (>20 m $s^{-1}$) on 8–9 August, 2009. Winds from the SW would tend to move water away from the coast and prevent downwelling.

the outer shelf and along the canyon thalweg in October 2009 show distinct, physically stratified surface layers of 3–12 cm thickness, which were not present in the cores collected during January 2007 (Figs. 3–6). The canyon cores display this surface layer as physically laminated and with lower bulk density than the underlying material. Furthermore, the surface layer shows no evidence of the bioturbation seen in underlying layers, suggesting that the material was deposited by an event shortly before collection.

Consistent with the observed physical structures, each core analyzed from the October 2009 cruise shows a surface layer of uniformly low $^{210}$Pb activity. This layer is distinctly thicker in the cores from the canyon (915-s.09, 915–8, 915–9; Figs. 3–6) than in the core collected from the outer shelf (915-MV; Fig. 7). As seen in Figs. 3–6, the $^{210}$Pb activities decrease upward within the surface layer, from activities of 10–20 dpm $g^{-1}$, to activities of only 2–3 dpm $g^{-1}$. Activities just below the base of the layer (as identified by x-radiographs) are consistent with activities at the surface of the 2007 cores. The x-radiographs show a very sharp transition downward between the surface layer and pre-existing sediment. The $^{210}$Pb activities reveal a more gradual transition within the surface layer to levels in the pre-existing layer. The explanation is not clear, but might reflect a mixture of new riverine sediment (low $^{210}$Pb activity) and recent shelf and canyon sediment (some $^{210}$Pb activity) that becomes progressively more dominated by riverine sediment as the river flood progresses (similar to observations in Eel canyon; Mullenbach and Nittrouer, 2000).

Grain-size analysis supports the hypothesis that the surface layer is a flood deposit derived from river sediment, based on an increase of the clay fraction (Figs. 3–6), as seen in previous studies (e.g., Sommerfield et al., 1999; Leithold and Hope, 1999; Leithold and Blair, 2001). In Fangliao Canyon, clay percentages within the 2009 surface deposits are as much as 2–4 times greater than in the underlying strata. The increase in clay fraction precludes the possibility of grain-size variation being responsible for the decreased surface $^{210}$Pb activity, and is consistent with observations of river floods in other similar situations (e.g., Eel River, Sommerfield et al., 1999; Po River, Palinkas et al., 2005; Waiapu River, Kniskern et al., 2001).

The $\delta^{13}$C values for the surface flood layers have the smallest values found in each core (~25.50‰, Fig. 7), plotting near the terrestrial end member (−25.5‰, Fig. 8a). Samples below the flood deposit exhibit $\delta^{13}$C values closer to −22.00‰, compositions that are significantly

enriched in marine organic carbon (Student's $t$-test, $p<0.001$) and thus, relative to underlying material, the surface sediment has a stronger terrestrial carbon signature. The relatively high N:C ratios of the surface samples further suggest they are composed of terrestrial soil, while the lower N:C ratios for the coarse and deep horizons suggest that vascular plant debris (i.e., material from the land surface) enters the canyon during other, less dramatic, river discharge conditions. This vascular plant debris is also from soil, but undergoes significant dilution and replacement by marine carbon (e.g. Keil et al., 1997). In other sedimentological studies (e.g. Sommerfield et al., 1999), $^{7}$Be has been used as an identifier of terrestrial origin; however, it was not observed in the flood layer in this study, as we will discuss in a following section. For this environment, the geochemical tracers were necessary to determine the provenance of the flood layer.

Comparisons of x-radiograph images, $^{210}$Pb profiles, grain-size distributions, and $\delta^{13}$C values from January 2007 and October 2009 provide strong evidence that an event shortly before the 2009 cruise (i.e., Typhoon Morakot) generated a distinct flood layer that records the signatures of terrestrial sediment origin. Examination of the nearby riverine source or sources should help constrain the possible mechanisms for delivering this flood layer (hereafter referred to as "the Morakot deposit") to the canyon.

### 5.2. Accumulation without a point source

As described in Section 5.1, Typhoon Morakot deposited a flood layer of ~10 cm thickness in Fangliao Canyon. This might not be surprising, given that Typhoon Morakot was an extraordinarily wet storm (>270 cm precipitation in high-mountain regions). However, an examination of hydrograph data for nearby rivers suggests that no likely point source exists to deliver such a mass of sediment to the canyon seabed. A conservative estimate suggests that the Morakot deposit within the canyon (30 km long × 2 km wide × 0.1 m thick, 50% porosity, 2650 kg m$^3$ density) contains ~8 Mt of sediment. To approximate the suspended-sediment concentration necessary to deliver this mass of sediment, we applied the peak discharge rate from the largest measured tributary (3000 m$^3$ s$^{-1}$, Linbian River; Table 2) to a 24-h period. This analysis suggests that a suspended-sediment concentration of ~30 g l$^{-1}$ would be required to form the Morakot deposit. This estimate is especially conservative when considering visual observation during the October 2009 cruise, of a meters-thick flood deposit near the head of the canyon, which was too soft to sample with the box corer. Furthermore, this estimate requires that all river discharge flow directly to the canyon thalweg, which is unlikely considering the distance from the river mouth to the canyon head. Instead, using maximum theoretical discharges for all surrounding rivers (after Matthai, 1990; Table 2) located between ~15 km to the NW and ~25 km to the SE of the canyon head, and still assuming direct delivery to the canyon, each river would be required to carry ~3 g l$^{-1}$.

The fluvial drainage basins surrounding Fangliao Canyon to the north and east have areas ~20 km$^2$ to 300 km$^2$, and maximum possible water discharges (as calculated based on Matthai, 1990) of ~1300–6400 m$^3$ s$^{-1}$ (Table 2). The Gaoping River has been included (in Table 2) for relative scale, and is 1–2 orders of magnitude larger in both basin area and measured discharge than any nearby river. Furthermore, the Gaoping and Donggang Rivers have a direct connection to the head of Gaoping Canyon, but there is no such connection between the Fangliao and any of its surrounding rivers (Fig. 1). Rather than a single point source, it appears possible and likely that discharges from a line source of small mountainous rivers coalesced, resulting in the large supply of sediment into Fangliao Canyon.

The energetic oceanic conditions during peak discharge may have assisted the down canyon transport of water and sediment. Surface winds were from the west during the period of peak discharge, which would result in the net southward transport of surface waters through Ekman flow, and would not produce conditions favorable for downwelling. However, the relatively long wave periods (~12 s) indicate that wavelengths were on the order of hundreds of meters, and therefore that the surface gravity waves could have impacted the bottom to depths of ~100 m (Komar et al., 1972; Pond and Pickard, 1983). Consequently, wave energy could have resuspended shelf material and/or caused liquefaction and failures (e.g., slumping), all of which could have initiated flow down canyon.

Without additional samples or direct observation of the responsible process, distinguishing the mechanism of sediment delivery is difficult. Furthermore, while our estimate of riverine suspended-sediment concentration (SSC) suggests that hyperpycnal plumes were not necessary to form the Morakot deposit, we do have measured SSC from the Liwu River in northeast Taiwan, which shows that hyperpycnal concentrations (>90 g l$^{-1}$ in this case) were achieved at an area of the island less impacted by rainfall (Fig. 10). Based on our observations of the Morakot deposit, we can consider its delivery to be initiated by one of the following processes:

a) river suspended-sediment concentrations >40 g l$^{-1}$ flowing directly from the surrounding rivers as hyperpycnal plumes;
b) terrestrial material from rivers depositing rapidly on the outer shelf, until cyclic loading from storm waves generated slumps; or,
c) terrestrial material from rivers mixing with shelf material resuspended by storm waves, and generating a wave-supported fluid mud (>10 g l$^{-1}$).

Of these possibilities, we believe the third option (c) is the most likely. Coalescence of the discharges from several sources into a single hyperpycnal flow with no input of previously existing shelf material would be unlikely, given the energetic nature of the shelf during a typhoon. While slumping of material that accumulated around the canyon head cannot be ruled out, this does not explain the gradient in $^{210}$Pb activities at the base of the Morakot deposit.

### 5.3. Sediment accumulation rates in Fangliao Canyon

An examination of the radiochemical and geochemical data suggests that significant volumes of sediment are delivered to Fangliao

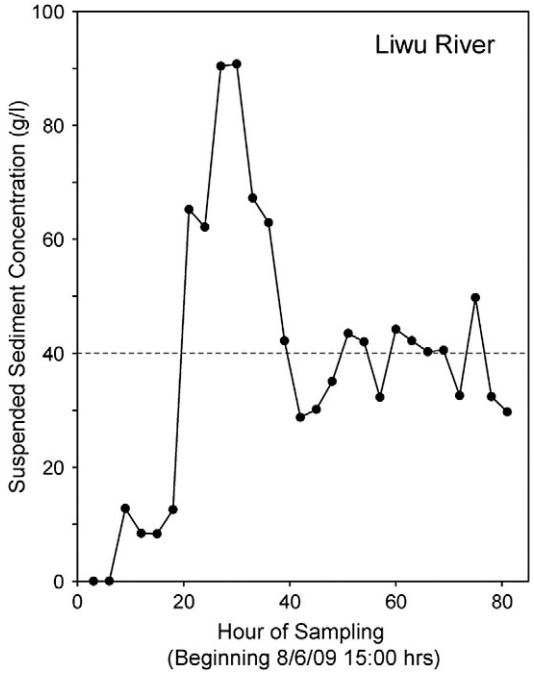


**Fig. 10.** Liwu River suspended-sediment concentration during Typhoon Morakot. Samples were collected every 3 h from a bridge ~5 km upstream of the river mouth. The Liwu River appears to have reached hyperpycnal concentrations (>40 g l$^{-1}$) after ~20 h, and remained at or near this concentration for the next several days.

Canyon on a regular basis. We see from several cores that excess $^{210}$Pb activity is observed 40–50 cm below the seabed surface in the canyon. We cannot calculate absolute accumulation rates because the profiles indicate rapid and non-steady-state sedimentation. However, because $^{210}$Pb shows no appreciable decrease (i.e., decay of <1 half-life, or 22.3 years), we can estimate minimum accumulation rates >2 cm year$^{-1}$ (e.g., core 915-s.09).

The $\delta^{13}$C, N:C, Ad/Al, and C/V data allow establishment of three general sedimentation regimes from these cores (Figs. 7 and 8). The material in the Morakot deposit (surface layer) appears to be mildly degraded terrestrial material, indicative of soil erosion. A high Ad/Al ratio suggests digestion of aldehydes into acids, the low $\delta^{13}$C value approaches the terrestrial end member, and the N:C versus $\delta^{13}$C relationship places the surface material firmly in the realm of soil, as described by Keil et al. (1994) and Rezende et al. (2010). Below the surface layer of 2009 cores is a sandy layer that contains less terrestrial organic material, possibly representing shelf material carried into the canyon and diluted by additions of marine carbon. One suggestion by Hsu et al. (2008) is that this sandy layer was transported via earthquake-generated slumping associated with the Pingtung earthquake in December 2006. Below the coarse layer, we see sediment that has Ad/Al and C/V ratios similar to the surficial Morakot deposit, but with an enriched $\delta^{13}$C ratio. This implies that under less-energetic conditions than the flood event, soil is brought to the ocean by rivers where it mixes with oceanic carbon before reaching the canyon. Even if we ignore the Morakot deposit of >10 cm from a single event, areas within the canyon thalweg (e.g. 915-s.09) are still accumulating sediment with a terrestrial signature at a rate >2 cm year$^{-1}$.

### 5.4. $^{7}$Be in SW Taiwan

Typically, $^{7}$Be (half-life 53 days) presence is used as an indicator of whether a flood deposit has been recently derived from a terrestrial source (e.g., Sommerfield et al., 1999). The lack of $^{7}$Be in cores from all depths in Fangliao Canyon and from the adjacent shelf could suggest that the surface layers were generated from older material (supplied >6 months before collection). However, the Liwu River provides a valuable lesson for discharge of Taiwanese rivers during a storm. Sediments collected from the Liwu contained no $^{7}$Be, despite measured suspended-sediment concentrations in excess of 90 g l$^{-1}$ (Fig. 10). Similarly, cores from nearby Gaoping Canyon (which is suspected of hyperpycnal flow during previous storms of lower discharge; Huh et al., 2009) are devoid of $^{7}$Be, even in flood deposit samples containing root fragments. Furthermore, the $\delta^{13}$C signature of samples from within the Fangliao Canyon surface layer shows a strong terrestrial signal (~−25.00‰). Thus, it is possible that $^{7}$Be is not always an effective tracer of flood deposits in Taiwan. The local morphology and climate provide a couple of explanations. One possibility is that because the deeply incised, small mountainous river basins have little surface area to accumulate $^{7}$Be, surface sediment is a very small fraction of the total sediment removed from the land, significantly diluting any $^{7}$Be signal. This is supported by the geochemical evidence, which shows that the organic matter delivered to Fangliao Canyon during Morakot is more similar to soil (suggesting deeper erosion), as opposed to vascular plant debris (which would be found on the land surface). The other possible reason is that the frequent storms regularly remove $^{7}$Be in surface soils, and not enough time passes between storms for the deposition of significant amounts of new $^{7}$Be.

Based on evidence from x-radiographs, $^{210}$Pb activities, grain-size distributions, $\delta^{13}$C values, and the degraded nature of the organic matter, we conclude that the ~10 cm thick surficial deposits created by Typhoon Morakot are comprised of terrestrial material largely supplied by typhoon flooding, despite the absence of $^{7}$Be.

## 6. Summary

Typhoon Morakot devastated Taiwan with days of intense rainfall and strong winds. The precipitation caused the small, mountainous rivers that drain Taiwan to flood, reaching peak discharges on 8–9 August 2010. Cores collected during a cruise to Fangliao Canyon 7 weeks later reveal a ubiquitous surface deposit, ~3–12 cm thick, despite the lack of connection between the canyon head and a significant river source. Based on the canyon dimensions and the deposit porosity and thickness, we estimate that the surrounding rivers debouched at least 8 Mt of sediment into Fangliao Canyon. The material formed a surface layer with strongly terrestrial geochemical and radioisotopic signatures, and with distinct physical stratification in x-radiographs. While the exact mechanism for delivering this material from its terrestrial source to its canyon sink is unclear, this evidence suggests that some sort of gravity flow is responsible. Despite the terrestrial source and rapid sampling, the flood layer is devoid of $^{7}$Be, suggesting that in some instances and regions characterized by deep stream incision, $^{7}$Be is not found as a signature of recent terrigenous input.

## Acknowledgements

The authors thank Saulwood Lin, Chi-Chieh Su, Shuh-Ji Kao, Chih-An Huh, Cheng-Shing Chang, and Ben Sheets for their assistance with data collection and analysis. We also thank the crew of the R/V Ocean Researcher I for their assistance in both the 2007 and 2009 cruises. This work was funded by the U.S. National Science Foundation and the National Science Council of Taiwan, through the NSF-EAPSI 0914272.

## References

Adams, J., 1984. Active deformation of the Pacific northwest continental margin. Tectonics 3, 449–472.
Chang, J.C., 1983. Stream order and stream net ratios of drainage basins in Taiwan. PhD Thesis, University of Tsukuba, Tsukoba, 12 pp.
Chiang, C.S., Yu, H.S., 2008. Evidence of hyperpycnal flows at the head of the meandering Kaoping Canyon off SW Taiwan. Geo-Marine Letters 28, 161–169.
Coakley, J.P., Syvitski, J.P.M., 1991. SediGraph technique. In: Syvitski, J.P.M. (Ed.), Principles, Methods and Application of Particle Size Analysis. Cambridge University Press, Cambridge, pp. 129–142.
Dadson, S., Hovius, N., Pegg, S., Dade, W.B., Horng, M.J., Chen, H., 2005. Hyperpycnal river flows from an active mountain belt. Journal of Geophysical Research 110, F04016.
DeGeest, A.L., Mullenbach, B.L., Puig, P., Nittrouer, C.A., Drexler, T.M., Durrieu du Madron, X., Orange, D.L., 2008. Sediment accumulation in the western Gulf of Lions, France: the role of Cap de Creus Canyon in linking shelf and slope sediment dispersal systems. Continental Shelf Research 28, 2031–2047.
Degens, E.T., 1969. Biogeochemistry of stable carbon isotopes. In: Eglinton, G., Murphy, M.T.J. (Eds.), Organic Geochemistry. Springer, New York, pp. 304–329.
Doong, D.J., Chuang, L.Z.H., Kao, C.C., Lin, Y.B., Jao, K.C., 2009. Statistics of buoy-observed waves during typhoons at Taiwanese waters from 1997 to 2008. OCEANS 2009, MTS/IEEE Biloxi – Marine Technology for our future: global and local challenges, Biloxi, MS, pp. 1–7.
Drake, D.E., 1999. Temporal and spatial variability of the sediment grain-size distribution on the Eel shelf: the flood layer of 1995. Marine Geology 154, 169–182.
Dukat, D.A., Kuehl, S.A., 1995. Non-steady-state $^{210}$Pb flux and the use of $^{223}$Ra/$^{226}$Ra as a geochronometer on the Amazon continental shelf. Marine Geology 125, 329–350.
Goldfinger, C., Nelson, C.H., Johnson, J.E., 2003. Holocene earthquake records from the Cascadia subduction zone and northern San Andreas fault based on precise dating of offshore turbidites. Annual Review of Earth and Planetary Sciences 31, 555–577.
Goni, M.A., Hedges, J.I., 1990. Potential applications of cutin-derived CuO reaction products for discriminating vascular plant sources in natural environments. Geochimica et Cosmochimica Acta 42, 3073–3081.
Hedges, J.I., 1976. Land-derived organic matter in surface sediments from the Gulf of Mexico. Geochimica et Cosmochimica Acta 40, 1019–1029.
Hedges, J.I., Mann, D.C., 1979. The characterization of plant tissues by their lignin oxidation products. Geochimica et Cosmochimica Acta 43, 1803–1807.
Hilton, R.G., Galy, A., Hovius, N., 2008. Riverine particulate organic carbon from an active mountain belt: The importance of landslides: Global Biogeochemical Cycles 22, p. GB1017.
Hsu, S.K., Kuo, J., Lo, C.L., Tsai, C.H., Doo, B.D., Ku, C.Y., 2008. Turbidity currents, submarine landslides and the 2006 Pingtung earthquake off SW Taiwan. Terrestrial, Atmospheric, and Ocean Sciences 19, 767–772.
Huh, C.A., Liu, J.T., Lin, H.L., Xu, J.P., 2009. Tidal and flood signatures of settling particles in the Gaoping submarine canyon (SW Taiwan) revealed from radionuclide and flow measurements. Marine Geology 267, 8–17.

Jaeger, J.M., Nittrouer, C.A., Scott, N.D., Milliman, J.D., 1998. Sediment accumulation along a glacially impacted mountainous coastline: Northeast Gulf of Alaska. Basin Research 10, 155–173.
Kao, S.J., Dai, M., Selvaraj, K., Zhai, W., Cai, P., Chen, S.N., Yang, J.Y.T., Liu, J.T., Liu, C.C., Syvitski, J.P.M., 2010. Cyclone-driven deep sea injection of freshwater and heat by hyperpycnal flow in the subtropics. Geophysical Research Letters 37, L21702.
Kao, S.J., Liu, K.K., 2000. Stable carbon and nitrogen isotope systematic in a human-disturbed watershed (Lanyang-Hsi) in Taiwan and the estimation of biogenic particulate organic carbon and nitrogen fluxes. Global Biogeochemical Cycles 14, 189–198.
Kao, S.J., Milliman, J.D., 2008. Water and Sediment Discharge from Small Mountainous Rivers, Taiwan: The Roles of Lithology, Episodic Events, and Human Activities. The Journal of Geology 116, 431–448.
Keil, R.G., Tsamakis, E., Fuh, C.B., Giddings, J.C., Hedges, J.I., 1994. Mineralogical and textural controls on the organic composition of coastal marine sediments: hydrodynamic separation using SPLITT-fractionation. Geochimica et Cosmochimica Acta 58, 879–893.
Keil, R.G., Mayer, L.M., Quay, P.D., Richey, J.E., Hedges, J.I., 1997. Loss of organic matter from riverine particles in deltas. Geochimica et Cosmochimica Acta 61 (7), 1507–1511.
Keil, R.G., Tsamakis, E., Giddings, J.C., Hedges, J.I., 1998. Biochemical distributions among size-classes of modern marine sediments. Geochimica et Cosmochimica Acta 62 (8), 1347–1364.
Kineke, G.C., Woolfe, K.J., Kuehl, S.A., Milliman, J.D., Dellapenna, T.M., Purdon, R.G., 2000. Sediment export from the Sepik River, Papual New Guinea: evidence for a divergent sediment plume. Continental Shelf Research 20, 2239–2266.
Kniskern, T.A., Kuehl, S.A., Harris, C.K., 2001. Sediment accumulation patterns and fine-scale strata formation on the Waiapu River shelf, New Zealand. Marine Geology 270, 188–201.
Komar, P.D., Neudeck, R.H., Kulm, L.D., 1972. Observations and significance of deep-water oscillatory ripple marks on the Oregon continental shelf. In: Swift, D.J.P., Duane, D.B., Pilky, O.R. (Eds.), Shelf Sediment Transport. Dowde, Hutchinson, and Ross, Inc., Stroudsburg, PA, pp. 601–619.
Kudrass, H.R., Michels, K.H., Wiedicke, M., Suckow, A., 1998. Cyclones and tides as feeders of a submarine canyon off Bangladesh. Geology 26, 715–718.
Lang, S., 2009. NASA's TRMM satellite sees typhoon Morakot's massive flooding in Taiwan. NASA – hurricane season 2009. NASA, Morakot. [Online]. Available: http://www.nasa.gov/mission_pages/hurricanes/archives/2009/h2009_Morakot.html. [2009, August 30].
Lee, H.J., Locat, J., Desgagnés, P., Parsons, J.D., McAdoo, B.G., Orange, D.L., Puig, P., Wong, F.L., Dartnell, P., Boulanger, E., 2007. Submarine Mass Movements on Continental Margins. In: Nittrouer, C.A., Austin, J.A., Field, M.E., Kravitz, J.H., Syvitski, J.P.M., Wiberg, P.L. (Eds.), Continental Margin Sedimentation: From Sediment Transport to Sequence Stratigraphy. Blackwell Publishing Ltd., Oxford, UK, pp. 213–274.
Leithold, E.L., Blair, N.E., 2001. Watershed control on the carbon loading of marine sedimentary particles. Geochimica et Cosmochimica Acta 65, 2231–2240.
Leithold, E.L., Hope, R.S., 1999. Deposition and modification of a flood layer on the northern California shelf: lessons from and about the fate of terrestrial particulate organic carbon. Marine Geology 154, 183–195.
Liu, J.T., Lin, H.L., 2004. Sediment dynamics in a submarine canyon: a case of river-sea interaction. Marine Geology 207, 55–81.
Liu, C.S., Huang, I.L., Teng, L.S., 1997. Structural features off southwestern Taiwan. Marine Geology 137, 305–319.
Liu, J.T., Liu, K.J., Huang, J.C., 2002. The effect of a submarine canyon on the river sediment dispersal and inner shelf sediment movements in southern Taiwan. Marine Geology 181, 357–386.
Liu, J.T., Lin, H.L., Hung, J.J., 2006. A submarine canyon conduit under typhoon conditions off Southern Taiwan. Deep Sea Research 53, 223–240.
Liu, J.T., Hung, J.J., Lin, H.L., Huh, C.A., Lee, C.L., Hsu, R.T., Huang, W.T., Chu, J.C., 2009. From suspended particles to strata: the fate of terrestrial substances in the Gaoping (Kaoping) submarine canyon. Journal of Marine Systems 76, 417–432.
Malouta, D.N., Gorsline, D.S., Thornton, S.E., 1981. Processes and rates of Recent (Holocene) basin filling in an active transform margin; Santa Monica Basin, California continental borderland. Journal of Sedimentary Research 51, 1077–1095.
Marshall, N.F., 1978. Large storm-induced sediment slump reopens an unknown Scripps Submarine Canyon tributary. In: Stanley, D.J., Kelling, G. (Eds.), Sedimentation in Submarine Canyons, Fans and Trenches. Dowden, Hutchinson and Ross, Stroudsburg, PA, pp. 73–84.
Matthai, H.F., 1990. Floods. In: Wolman, M.G., Riggs, H.C. (Eds.), The Geology of North America Vol. 0–1, Surface Water Hydrology. Geological Society of America, Boulder, CO, pp. 97–120.
Milliman, J.D., Kao, S.J., 2005. Hyperpycnal discharge of fluvial sediment to the ocean: impact of super-typhoon Herb (1996) on Taiwanese rivers. Journal of Geology 113, 503–516.
Milliman, J.D., Meade, R.H., 1983. World-wide delivery of river sediment to the oceans. Journal of Geology 91, 1–21.
Mulder, T., Syvitski, J.P., 1995. Turbidity currents generated at river mouths during exceptional discharges to the world oceans. Journal of Geology 103, 285–299.
Mulder, T., Syvitski, J.P., Migeon, S., Faugustères, J.C., Savoye, B., 2003. Marine hyperpycnal flows: initiation, behavior, and related deposits. A review. Marine and Petroleum Geology 20, 861–882.
Mullenbach, B.L., Nittrouer, C.A., 2000. Rapid deposition of fluvial sediment in the Eel Canyon, northern California. Continental Shelf Research 20, 2191–2212.
Mullenbach, B.L., Nittrouer, C.A., Puig, P., Orange, D.L., 2004. Sediment deposition in a modern submarine canyon: Eel Canyon, northern California. Marine Geology 211, 101–119.
Nittrouer, C.A., Sternberg, R.W., 1981. The formation of sedimentary strata in an allocthonous shelf environment: the Washington continental shelf. Marine Geology 42, 201–212.
Nittrouer, C.A., Sternberg, R.W., Carpenter, R., Bennett, J.T., 1979. The use of $^{210}$Pb as a sedimentological tool: application to the Washington continental shelf. Marine Geology 31, 291–316.
Palinkas, C.M., Nittrouer, C.A., Wheatcroft, R.A., Langone, L., 2005. The use of $^{7}$Be to identify event and seasonal sedimentation near the Po River delta, Adriatic Sea. Marine Geology 222–223, 95–112.
Parsons, J.D., Friedrichs, C.T., Traykovski, P.A., Mohrig, D., Imran, J., Syvitski, J.P.M., Parker, G., Puig, P., Buttles, J.L., García, M.H., 2007. The Mechanics of Marine Sediment Gravity Flows. In: Nittrouer, C.A., Austin, J.A., Field, M.E., Kravitz, J.H., Syvitski, J.P.M., Wiberg, P.L. (Eds.), Continental Margin Sedimentation: From Sediment Transport to Sequence Stratigraphy. Blackwell Publishing Ltd., Oxford, UK, pp. 274–337.
Paull, C.K., Mitts, P., Ussler III, W., Keaten, R., Greene, H.G., 2005. Trail of sand in upper Monterey Canyon: Offshore California. GSA Bulletin 117, 1134–1145.
Pond, S., Pickard, G.L., 1983. Introductory Dynamical Oceanography. Butterworth-Heinemann Ltd, Oxford, UK.
Puig, P., Palanques, A., 1998. Temporal variability and composition of settling particle fluxes on the Barcelona continental margin (Northwestern Mediterranean). Journal of Marine Research 56, 639–654.
Puig, P., Ogston, A.S., Mullenbach, B.L., Nittrouer, C.A., Sternberg, R.W., 2003. Shelf-to-canyon sediment-transport processes on the Eel continental margin (northern California). Marine Geology 193, 129–149.
Puig, P., Ogston, A.S., Mullenbach, B.L., Nittrouer, C.A., Parsons, J.D., 2004. Storm-induced sediment gravity flows at the head of the Eel submarine canyon, northern California margin. Journal of Geophysical Research Letters 109, C03019.
Rezende, C.E., Pfeiffer, W.C., Martinelli, L.A., Tsamakis, E., Hedges, J.I., Keil, R.G., 2010. Lignin phenols used to infer organic matter sources to Sepetiba Bay – RJ, Brasil. Estuarine, Coastal and Shelf Science 87, 479–486.
Sarkanin, K.V., Ludvig, C.H., 1971. Lignins. Wiley-Interscience, New York.
Sommerfield, C.K., Nittrouer, C.A., Alexander, C.R., 1999. $^{7}$Be as a tracer of flood sedimentation on the northern California continental margin. Continental Shelf Research 19, 335–361.
Talling, P.J., Wynn, R.B., Mason, D.G., Frenz, M., Cronin, B.T., Schiebel, R., Akhmetzhanov, A.M., Dallmeier-Tiessen, S., Benetti, S., Weaver, P.P.E., Georgiopoulou, A., Zühlsdorff, C., Amy, L.A., 2007. Onset of submarine debris flow deposition far from original giant landslide. Nature 450, 541–544.
Traykovski, P., Geyer, W.R., Irish, J.D., Lynch, J.F., 2000. The role of wave-induced density-driven fluid mud flows for cross-shelf transport on the Eel River continental shelf. Continental Shelf Research 20, 2113–2140.
Walsh, J.P., Nittrouer, C.A., 2003. Contrasting styles of off-shelf sediment accumulation in New Guinea. Marine Geology 196, 105–125.
Walsh, E.M., Ingalls, A.E., Keil, R.G., 2008. Sources and transport of terrestrial organic matter in Vancouver Island Fjords and the Vancouver-Washington Margin: a multiproxy approach using $\delta 13C_{org}$, lignin phenols, and ether lipid BIT index. Limnology and Oceanography 53 (3), 1054–1063.
Warrick, J.A., Milliman, J.D., 2003. Hyperpycnal sediment discharge from semiarid southern California rivers: implications for coastal sediment budgets. Geology 31, 781–784.
Westerhausen, L., Poynter, J., Eglinton, G., Erlenkeuser, H., Sarnthein, M., 1993. Marine and terrigenous origin of organic matter in modern sediments of the equatorial East Atlantic: the σ13C and molecular record. Deep Sea Research Part I: Oceanographic Research Papers 40 (5), 1087–1121.
Wheatcroft, R.A., Borgeld, J.C., 2000. Oceanic flood deposits on the northern California shelf: large-scale distribution and small-scale physical properties. Continental Shelf Research 20, 2163–2190.
Wheatcroft, R.A., Wiberg, P.L., Alexander, C.R., Bentley, S.J., Drake, D.E., Harris, C.K., Ogston, A.S., 2007. Post-depositional alteration and preservation of sedimentary strata. In: Nittrouer, C.A., Austin, J.A., Field, M.E., Kravitz, J.H., Syvitski, J.P.M., Wiberg, P.L. (Eds.), Continental Margin Sedimentation: From Sediment Transport to Sequence Stratigraphy. Blackwell Publishing Ltd., Oxford, UK, pp. 101–155.
Wiberg, P.L., 2000. A perfect storm: formation and potential for preservation of storm beds on the continental shelf. Oceanography 13, 93–99.
Xu, J.P., Rosenfeld, L.K., 2004. In-situ measurements of velocity structure within turbidity currents. Geophysical Research Letters 31, L09311.